The Quantal Source of Area Supralinearity of Flash Responses in *Limulus* Photoreceptors

NORBERTO M. GRZYWACZ, PETER HILLMAN, and BRUCE W. KNIGHT

From the Institute of Life Sciences, The Hebrew University of Jerusalem, Jerusalem 91904, Israel, and The Rockefeller University, New York, New York 10021

ABSTRACT The time integrals of the responses of dark-adapted *Limulus* ventral photoreceptors to flashes exhibit a supralinear dependence on intensity at intermediate intensities. By decomposing the responses into their elementary single-photon components ("bumps"), we are able to calculate the overall quantum efficiency and to display the time courses of the bump amplitude and rate of appearance. Since the time course of the flash response is not slow compared with that of the bump, it was necessary, in order to carry out the decomposition, to develop a new technique for noise analysis of dynamic signals. This new technique should have wide applications. Our main finding is that the supralinearity of the flash responses corresponds to an increase in bump amplitude, with little change in bump duration or quantum efficiency. The time courses of the bump rate and of the change in bump amplitude are peaked and have widths similar to that of the response itself. The peaks of the time courses of the bump rate and amplitude displayed against the starting times of the bumps do not coincide and occur ~80 and ~40 ms, respectively, before the peak of the response. The time from the start of a bump to its centroid is ~70 ms, which means that the time at which the bump centroid reaches its maximum follows the response peak by 30 ms. These results impose constraints on possible mechanisms for the amplitude enhancement.

INTRODUCTION

Many photoreceptor cells respond to dim illumination with isolated slow potentials or "bumps," which can be identified as the responses to single photons (Fuortes and Yeandle, 1964; Lillywhite, 1977). These responses have been seen in the invertebrates *Limulus* (Yeandle, 1958; Millecchia and Mauro, 1969), locust (Scholes, 1965), fly (Kirschfeld, 1965; Wu and Pak, 1975), leech (Walther, 1965), spider (DeVoe, 1972), and *Hermissenda* (Takeda, 1982), and in the vertebrate toad (Baylor et al., 1979).

At very low light intensities, the rate of appearance of the bumps increases in proportion to light intensity (Fuortes, 1959; Adolph, 1964). At higher intensities, the bumps appear to merge, which suggests that the general receptor potential is a

Address reprint requests to Dr. Norberto M. Grzywacz, Center for Biological Information Processing, Massachusetts Institute of Technology, E25-201, Cambridge, MA 02139.

J. GEN. PHYSIOL. © The Rockefeller University Press · 0022-1295/88/05/0659/26 $2.00
Volume 91 May 1988 659–684

summation of these bumps (Rushton, 1961). If one assumes that the bumps are not so grossly modified by interaction as to lose their identity, one can decompose the signal into its elements by techniques of noise analysis (for a review, see Neher and Stevens, 1977). These techniques have been applied to the steady state responses of photoreceptors. When applied to species where individual bumps have not been seen, the analysis indicates the presence of bumps too small to be directly recorded by standard electrophysiological methods (Mauro et al., 1982). Thus, bumps appear to be fundamental to the process of phototransduction. The analysis also shows that the sublinear dependence of response amplitude on intensity, which is associated with light adaptation, arises primarily from a reduction in the bump amplitude, with relatively little change in the bump quantum efficiency or time course (Dodge et al., 1968; Wu and Pak, 1978; Wong and Knight, 1980; Wong et al., 1982).

Light adaptation is not the only nonlinearity that appears at physiological levels of light intensity. A cell sensitization that manifests itself as an enhancement of the amplitude of the response to flashes of light can appear as a consequence of prior or simultaneous conditioning light. This phenomenon has been seen in the invertebrates barnacle (Hanani and Hillman, 1976; Ventura and Puglia, 1977) and *Limulus* (Fein and Charlton, 1977), and, in the presence of phosphodiesterase inhibitors, in the vertebrate toad (Capovilla et al., 1983). At very low intensities, where individual bumps can be examined, Stieve and Bruns (1980, 1983) observed in *Limulus* a light-induced increase in bump amplitude and quantum efficiency. This sensitization may be related to the supralinear dependence on intensity of the amplitude of the responses of dark-adapted cells to flashes, in *Limulus* (Brown and Coles, 1979) and in toad (Yau et al., 1981; Capovilla et al., 1983).

In this article, we will concentrate on the supralinearity phenomenon in *Limulus*. Because this phenomenon has been seen only in transient signals, it could not be analyzed by standard stochastic noise-analysis techniques. Sigworth (1980, 1981*a*, *b*) generalized the steady state techniques to transient signals whose noisy nature is due to the random opening and closing of ionic channels. His methods are appropriate for rectangular unitary signals. In the present article, we develop a method for handling more general unitary time courses. We have applied this methodology to appropriate experiments in order to determine the quantal correlates of the supralinearity in *Limulus*.

THEORY

The development of the noise-analysis procedure for transient signals is parallel to that for the steady state, as presented, for example, by Wong and Knight (1980). The model has four assumptions: (*a*) that the signal $J(t)$ recorded at time t arises from a summation of elementary events that have begun at times t' prior to t; (*b*) that the appearance of the elementary events is a random Poisson process with a mean rate $\lambda(t')$; (*c*) that the elementary events have a common normalized waveform $g(t - t')$ (zero for $t - t' \leq 0$); and (*d*) that their amplitude $h(t')$ can change with time but that the temporal dependence of the amplitude is deterministic, and that the amplitude of an elementary event is a random variable whose probability density is determined only by its beginning time.

The first two assumptions are common in photoreception studies, but the other

two merit some inspection. Assumption *c* was made because steady state noise analysis shows a very weak dependence of the bump time course on light intensity over 5 log units of intensity. However, although the bump time course in fact does not change appreciably in the steady state, it might change in transient responses. Our experimental results give two lines of evidence that support the assumption that the bump time course in fact does not change very much. The first is the similarity of the bump calculated from noise analysis to the isolated bump observed in dim illumination. The second is the result of a method, to be described below, that shows that there are indeed no appreciable changes in the bump time course during the response.

In assumption *d*, the change in the amplitude h reflects a possible interaction among the chemical processes leading to the bump formation. Past fluctuation in the response could make the temporal behavior of h nondeterministic. Our assumption that h is deterministic to a good approximation conforms to the steady state analysis of the response of the ventral photoreceptor of *Limulus* (Wong et al., 1982). Wong et al. showed that in the steady state the bump amplitude depends strongly on the mean level of the preceding response but hardly at all on previous shot-noise fluctuations of the response.

An additional argument that can be brought against assumption *d* is that the size of the bump itself is a random variable (see Grzywacz and Hillman, 1985, and Laughlin and Lillywhite, 1982, for earlier references). We take into account the effects of the random nature of the bump amplitude by making deterministic the temporal behavior of the mean of the bump amplitude distribution. Grzywacz and Hillman (1985) found the bump area distribution to be exponential in continuous low-intensity light. Since the flash intensities used here are quite low, we have assumed the same distribution to be applicable. With the assumption of a common normalized waveform *g*, this implies an exponential amplitude distribution as well.

Finally, assumption *d* states that the amplitude of the bump is determined only by its starting time. This is equivalent to assuming that the stage of the amplification process in which the bump amplitude is determined precedes the stages in which the time course is determined. This is a plausible but arbitrary assumption, and an analysis of the possible alternatives will be made in a future article.

In this article, we shall use a set of conventional normalizations that have proven convenient in past work. If a bump is described by the waveform $B(t)$ (with the physical dimension of nanoamperes), then we choose its amplitude h (in nanoamperes) as

$$h = \frac{\int dt[B(t)]^2}{\int dt[B(t)]}.$$

It is convenient to define the bump duration, T (milliseconds), as

$$T = \frac{[\int dtB(t)]^2}{\int dt[B(t)]^2},$$

which in turn leads to a normalized bump waveform, $g(t)$ (dimensionless),

$$g(t) = T\frac{B(t)}{\int dtB(t)}.$$

We note that for a rectangular waveform, h is in fact the physical height and T is the physical duration, while $g(t)$ has physical height unity. Given the four above assumptions, the mean, $R(t)$, and the variance, $V(t)$, over repetitions of the random response, $J(t)$, can be evaluated by straightforward generalization of the method of Rice (1944):

$$R(t) = \int_{-\infty}^{t} \lambda(t')h(t')\, g(t - t')\, dt', \tag{1}$$

$$V(t) = 2\int_{-\infty}^{t} \lambda(t')h^2(t')g^2(t - t')\, dt'. \tag{2}$$

(Here the factor of 2 follows from the assumed exponential amplitude distribution, for which $\langle h^2 \rangle = 2\langle h \rangle^2$.) For a derivation of all the important equations in this article, see the Appendix.

One can note the similarity of these results to the steady state Eqs. 1 and 2 in Wong and Knight (1980), where the difference is that there λ is constant and can be taken outside the integral. Recognizing the relationship of the mean and variance to the properties of the basic components of the signal (Campbell's theorem) is usually the first step in the standard techniques of noise analysis. The second step is to show that if one knows the time course, g, the variables λ and h can be determined from the noise. In the steady state case, this is easily seen. Here, λ and h are constant, and Eqs. 1 and 2 reduce to:

$$R = \lambda hT, \tag{3}$$

$$V = 2\lambda h^2 T, \tag{4}$$

which are Eqs. 5 and 6 in Wong and Knight (1980). Now we see that if we have an estimate of g, measurement of R and V yields values of h and λ. Similarly, Eqs. 1 and 2 are a pair of integral equations that can be solved for $\lambda(t)$ and $h(t)$. To illustrate with a simple example, if g is an exponential shot with time constant τ, direct calculation from Eqs. 1 and 2 yields:

$$\frac{1}{2}\left(\frac{R(t)}{\tau} + \frac{dR(t)}{dt}\right) = \lambda(t)h(t), \tag{5}$$

$$\frac{1}{2}\left(\frac{V(t)}{\tau} + \frac{1}{2}\frac{dV(t)}{dt}\right) = \lambda(t)h^2(t). \tag{6}$$

In this case, if one has an estimate of τ and values for the mean, the variance, and their time derivatives, which can be readily derived from the data, one can easily solve for $\lambda(t)$ and $h(t)$.

Eqs. 5 and 6 help us to see the first major difference between the steady state techniques of noise analysis and the transient techniques. In the steady state case, the statistical moments can be determined from values of the signal at different instants of a single extended trial. However, the distribution of a transient signal is time dependent and so are the statistical moments in Eqs. 5 and 6. Thus, in order to obtain statistical properties of the signal at a particular time, one must use many repeated trials (Wong et al., 1974; Sigworth, 1980).

We now set out a procedure for estimating $g(t)$ from the ensemble of flash

responses. The data are decomposed in such a way as to determine an equivalent power spectrum, the "decompound power spectrum," which is identical in shape to that of a time-homogeneous shot noise generated by bumps of the same shape as those comprising the flash responses.

For this purpose, one measures the time-dependent autocovariance, $K(t_1, t_2)$, of the signal, which is the product of the differences between the actual values of the signal, $J(t_1)$ and $J(t_2)$, and its mean values, $R(t_1)$ and $R(t_2)$, averaged over the different trials:

$$K(t_1, t_2) = \overline{(J(t_1) - R(t_1))(J(t_2) - R(t_2))}. \tag{7}$$

By using methods similar to those employed by Rice (1944) (see Appendix), one obtains:

$$K(t_1, t_2) = 2\int_{-\infty}^{\infty} \lambda(t')h^2(t')g(t_1 - t')g(t_2 - t')\,dt'. \tag{8}$$

A double Fourier transformation of Eq. 8 now leads to a function of two temporal angular velocities, $F(\omega, \theta)$. Concentrating on the pathway $\theta = -\omega$, however, one obtains:

$$F(\omega, -\omega) = 2\tilde{\lambda}h^2(0)|\tilde{g}(\omega)|^2, \tag{9}$$

where the tilde indicates a Fourier transform. This equation is parallel to that for the steady state system:

$$F(\omega) = 2\lambda h^2|\tilde{g}(\omega)|^2. \tag{10}$$

(This is Eq. 16 in Wong and Knight, 1980.) Note the similarity of F in Eqs. 9 and 10, both being proportional to $|g|^2$. Now $F(\omega, -\omega)$, which we call the decompound power spectrum of $J(t)$, can be calculated directly from the data. A practical means of doing so is provided by the double Fourier transform of Eq. 7 in pathway $\theta = -\omega$, which gives:

$$F(\omega, -\omega) = \overline{|\tilde{J}(\omega)|^2} - |\tilde{R}(\omega)|^2. \tag{11}$$

That is, the power in the noise at each frequency is the average, over the trials, of the power, minus the power of the average of the signal at that frequency. With the result of this measurement, Eq. 9 determines the normalized $g(t)$ by use of Wong and Knight's methods.

METHODS

The preparation used in this investigation was the ventral photoreceptor of *Limulus*. The experiments were performed in full in four cells. The morphology of this cell is well known (Calman and Chamberlain, 1982) and the methods for its isolation have been described (Clark et al., 1969). The lateral olfactory nerve was dissected out, and its enclosing blood vessel was removed. The connective tissue remaining in the cell was digested with 0.7–0.9% protease P5130 (Sigma Chemical Co., St. Louis, MO). After this treatment, the nerve was washed four times, mounted in a small Perspex chamber, and perfused with artificial seawater. The composition of the seawater was similar to that used by Bayer and Barlow (1978): 430 mM NaCl, 10 mM KCl, 10 mM $CaCl_2$, 20 mM $MgCl_2$, and 27 mM $MgSO_4$. It was buffered to pH 7.3

with 0.5 mM HEPES, 0.5 mM Tes (Sigma Chemical Co.), and a titration of NaOH (from a 3-M solution). The experiments were performed at room temperature (17–21°C).

The light source was a green light-emitting diode (LED) solid-state lamp (4958, Hewlett-Packard Co., Palo Alto, CA). This particular LED was chosen because of its high brightness and the fact that its peak wavelength, 565 nm, is near the maximum of the *Limulus* ventral eye action spectrum (Graham and Hartline, 1935; Adolph, 1968). The electronic control system for the LED was built by us according to Nygaard and Frumkes (1982). The control voltage for the LED was supplied by a computer (Apple II Europlus, Apple Computer Inc., Cupertino, CA) through an eight-bit A/D and D/A card (Mountain Computer Inc., Scotts Valley, CA). The timing was done either by the internal clock of the computer or by a digital timer (ES-8, AMP Instruments, Jerusalem). The light from the LED was carried into a shielded cage through a 0.5-mm fiber optic bundle (American Optical Co., Buffalo, NY). The tip of the optic bundle was placed near the impaled cell. The intensity of the light source was attenuated by means of neutral-density filters. The unattenuated light intensity elicited $\sim 10^5$ bumps/s in sensitive photoreceptors.

The ventral photoreceptor of *Limulus* has regenerative properties (Millecchia and Mauro, 1969). These properties are a consequence of voltage-dependent currents that appear when the cell is depolarized (Fain and Lisman, 1981; Lisman et al., 1982). In order to avoid this complication, the experiments were performed with the cells voltage-clamped at their resting potentials (−40 to −65 mV). We used the classic two-electrode voltage-clamp technique (Katz and Schwartz, 1974; Smith et al., 1980). Under voltage clamp, the cell could be considered isopotential (Brown et al., 1979). The microelectrodes were filled with 4 M KCl (DC resistance, 20–40 MΩ) and connected to the voltage-clamp system with Ag/AgCl electrodes.

The voltage-clamp system had two modes of operation. In the first, the two electrodes recorded the membrane potential with respect to the bathing solution, whose potential was held at virtual ground. The cells that were accepted for study showed the same resting potential in both electrodes, the same response amplitude (to within 1 mV) to bright light, and completely correlated bumps.

The second mode of operation was the voltage-clamp mode. In this mode, the clamping amplifier supplied to one of the electrodes the current necessary to keep the membrane potential equal to the controlling level. The current was measured by a virtual-ground operational amplifier that worked in a current-to-voltage converter mode (1 nA/1 mV). The system could supply up to 1.5 μA. Tested on an artificial cell with passive electrical characteristics similar to those of the photoreceptor cells (an input resistance of 10 MΩ and a capacitance of 1 nF; Brown and Coles, 1979), the system responded to a 10-mV step change in the command voltage by reaching its final state (within noise) in <50 μs. The capacitive coupling between the two microelectrodes was reduced by connecting to ground an aluminum shield around the current microelectrode, connecting an aluminum shield around the voltage electrode to the feedback control signal through a large capacitor, using only a minimum depth of solution covering the cell, and spacing the two microelectrodes as far apart as possible (Smith et al., 1980).

The signal out of the voltage-clamp system was first amplified by an oscilloscope (RM 502A, Tektronix, Inc., Beaverton, OR) and then filtered. The major frequency components of interest in the biological signal lie below 20 Hz. The high-frequency components of the instrumental noise were filtered out with a two-pole Bessel low-pass filter with half-power point at 70 Hz, and by a band-rejection filter at 50 Hz, with a quality factor of 3. The half-power point of the total filter system was ~40 Hz. In Fig. 1, one can compare the residual instrumental noise from the artificial cell cited above with the biological noise typical in the experiments. The trace shows the instrumental noise. The lines indicate the size of the smallest digitizing bin used in this work. Practically all the instrumental noise falls within this lowest bin.

The graph shows the smallest biological variance recorded in the present work as a function of time after a flash at $t = 0$. Clearly, the instrumental noise in the present work is small and can be neglected.

The data were collected by the same Apple computer that controlled the stimulus. The A/D system could accept ±5 V, and a limiter for these voltages was installed at the input of the computer, preventing crosstalk between the A/D and D/A channels, which appeared when the input exceeded ±8 V. The computer sampled the signals at 39.1-μs intervals, and the average of 128 such consecutive samples was stored on a floppy disk. This procedure corresponds to a sampling rate of 200 Hz and was chosen to minimize the problem of aliasing as well as to provide further high-frequency filtering.

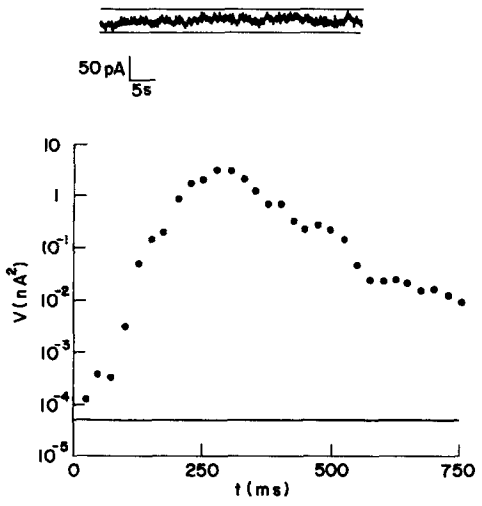

FIGURE 1. The instrumental noise. In the upper part of the figure is an example of the instrumental noise. This noise was recorded in an artificial (RC) cell with parameters $R = 10$ MΩ and $C = 1$ nF, similar to those of the biological cell. The trace is from a pen recorder (model 2200, Gould Inc., Cleveland, OH). The lines above and below the trace mark the smallest bin used in the computer during the course of this research, showing that the instrumental noise falls entirely within one bin. The dots in the lower figure are the logarithms of the smallest biological variance recorded after a short flash of light at $t = 0$ in cell 1 at intensity I_1 (cell numbers refer to Fig. 9). For comparison, the instrumental variance is shown as a horizontal straight line. Note that the biological variance is much higher than the instrumental, the difference reaching almost five decades at its maximal point.

After successful cell penetration, the photoreceptor was allowed to dark-adapt for 30 min. Then very low-intensity, 5-ms flashes of light were presented to the cell and the intensity was found, which resulted in about two bumps per flash; we call this intensity I_0. The experiment then consisted of repeated sets of three runs. 2 s before each run, 256 points (or 1.28 s) were averaged for use as a baseline. In each run, 10 flashes of light were delivered at 30-s intervals, the time needed for dark adaptation after each flash (Brown and Coles, 1979). The number of points recorded after a flash was 256, and the response never lasted more than 150 points. In the first run, the light intensity was I_0, in the second, 1 log unit higher (I_1), and in the third, 1.5 log units higher than I_0 ($I_{1.5}$).

After the experiment, the average response amplitude was calculated across each run. In most cells, the average amplitude for a given light intensity rose slightly with the run number

and then stabilized and finally declined. The first rising phase may be a continuation of dark adaptation and cell recovery from dissection, and the final falling phase is a consequence of the deterioration of the cell. Usually the stable period lasted ~90 min (three to four sets) and our final analysis was done only for this period.

At the I_0 intensity, most of the bumps were isolated, and we extracted four kinds of information: (*a*) the average time course of ~10 consecutive, clearly visible and isolated bumps, with their times of steepest rise made to coincide; (*b*) the average of the amplitudes h of isolated bumps, where h is defined above; (*c*) the mean number of bumps that appeared at this intensity; and (*d*) the mean total area (time integral) of the response. In the absence of illumination, spontaneous bumps appear (Yeandle and Spiegler, 1973). In our experiments, their rate was ~0.1 s^{-1} and their contribution to the area at low intensities was only ~2%. This contribution was even smaller at higher intensities.

For higher intensities, we extracted five kinds of information: (*a*) the time course, $g(t)$, of the bump as calculated from the decompound power spectrum; (*b*) the mean amplitude, $h(t)$, of the bump as a function of time as extracted from our generalized Campbell's theorem; (*c*) the rate, $\lambda(t)$, of the bumps as function of time, again from Campbell's theorem; (*d*) the mean total area of the response; and (*e*) the total number, N, of bumps elicited by the flash. The last number is obtained by time-integrating the rate of the bumps:

$$N = \int_0^\infty \lambda(t)\, dt. \tag{12}$$

In order to estimate the bump time course, $g(t)$, we make use of the decompound power spectrum $F(\omega, -\omega)$ (see Eqs. 9 and 11). We determined $F(\omega, -\omega)$ by Eq. 11. For a given intensity, we first calculated the square of the absolute value of the Fourier transform of each response. We then averaged over the different trials. From this result, we subtracted the square of the absolute value of the Fourier transform of the mean response as taken from the different trials. The result of the subtraction is $F(\omega, -\omega)$. The Fourier transforms were performed by the classic FFT algorithm (Cooley and Tukey, 1965). We call attention to the fact that the decompound power spectrum has dimensions different from the usual power spectrum. This is because the decompound spectrum is a double Fourier transform of the autocovariance function, while the usual power spectrum is a single transform. The dimension of the usual spectrum is amperes squared times seconds, and that of the decompound spectrum is amperes squared times seconds squared, or coulombs squared. Having $F(\omega, -\omega)$ in hand, we used Eq. 9 to estimate g by the first method of Wong and Knight (1980). They chose for g a simple analytic form:

$$g(t) = \frac{2^{2n+1}(n!)}{(2n)!}\left(\frac{t}{\tau}\right)^n e^{-t/\tau}. \tag{13}$$

They pointed out that in these conditions the normalized decompound power spectrum, as calculated from Eq. 9, is:

$$\frac{F(\omega, -\omega)}{F(0, 0)} = \frac{1}{[1 + (\omega\tau)^2]^{n+1}}. \tag{14}$$

The parameters n and τ can be evaluated by fitting the right side of Eq. 14 to the experimental decompound power spectrum in scaled form in the following way. From Eq. 14 one obtains:

$$\log \frac{F(\omega, -\omega)}{F(0, 0)} = -(n + 1) \log \left(1 + (\omega\tau)^2\right), \tag{15}$$

which for a given n is a universal curve in log ω, which is only shifted to the right or left by changes in τ. We prepared templates for n from 1 to 10 and looked for the best fit of these templates to the experimental log $\left(F(\omega, -\omega)/F(0, 0)\right)$. This provides both n (from the best template) and τ (from the best shift), and determination of $g(t)$ follows from Eq. 13.

In order to verify whether there was any trend in the bump time course, we divided the flash responses into three equal sections for the low intensity and two for the high intensity. These were the largest numbers of sections into which it was possible to divide the response while keeping each section long compared with the bump duration. Making the approximation that each of these periods is long compared with the typical bump duration, the decompound power spectrum of the truncated responses as given by Eq. 11 is approximately (see Appendix):

$$F(\omega, -\omega) = \left(2\int\lambda(t')h^2(t')\,dt'\right)|\tilde{g}(\omega)|^2, \tag{16}$$

where the limits of the integral are, respectively, the beginning of the response and T' (the end of the first section), T' and T'' (the end of the second section), and T'' and the end of the response at the low intensity; and at the high intensity, respectively, the beginning and T', and T' and the end. This is again proportional to $|\tilde{g}(\omega)|^2$ and allows an estimation of $g(t)$. The approximation may be fairly coarse but this does not preclude us from concluding from an observed constancy of the calculated g that the bump time course is probably quite constant during the response.

The essential parameter of the bump time course is one that indicates its typical duration, T_{bump}. Referring to Eq. 13, it is:

$$T_{\text{bump}} = \frac{(n!)^2 2^{2n+1}\tau}{(2n)!}. \tag{17}$$

The mean amplitude, $h(t)$, and the rate, $\lambda(t)$, of the bumps as functions of time were calculated from Campbell's theorem by Eqs. 1 and 2. With $g(t)$ expressed as in Eq. 13, it is straightforward to calculate $\lambda(t)h(t)$ and $\lambda(t)h^2(t)$ in the same general manner as we did for the illustrative Eqs. 5 and 6. The repeated differentiation of Eqs. 1 and 2 yields:

$$\lambda(t)h(t) = \frac{(2n)!}{(n!)^2 2^{2n+1}} \sum_{i=0}^{n+1} \binom{n+1}{i} \tau^{i-1} \frac{d^i R}{dt^i} \tag{18}$$

$$\lambda(t)h^2(t) = \frac{(2n)!}{(n!)^2 2^{2n+3}} \sum_{i=0}^{2n+1} \binom{2n+1}{i} \left(\frac{\tau}{2}\right)^{i-1} \frac{d^i V}{dt^i}. \tag{19}$$

If τ is small enough, only the $i = 0$ term in the summations would have to be taken into account for the most interesting range of t. This would mean that the bump is so fast that we could do steady state noise analysis; no time derivatives at all would need to be taken. However, such an approximation is not adequate for our data, for which the response rise time may approach the bump duration. We therefore took the first two terms of Eqs. 18 and 19:

$$\lambda(t)h(t) = \frac{(2n)!}{(n!)^2 2^{2n+1}} \left[\frac{R}{\tau} + (n+1)\frac{dR}{dt}\right], \tag{20}$$

$$\lambda(t)h^2(t) = \frac{(2n)!}{(n!)^2 2^{2n+3}} \left[\frac{2V}{\tau} + (2n+1)\frac{dV}{dt}\right]. \tag{21}$$

In order to check this approximation, we postulated gamma-distribution functions for R and V, as in Eq. 13, with values for their constants close to those observed experimentally. With

these functions, the higher-derivative components in the sums in Eqs. 18 and 19 were found to contribute on the average no more than 5% to the summations in the range between the times where the response exceeded 10% of its maximum. About 98% of the area of the response was contained in this range.

To calculate R and V from the data, early baselines were subtracted. The derivatives were calculated by the standard five-point parabola approximation (Scheid, 1968). Since they were derived from quotients of numerical data, $h(t)$ and $\lambda(t)$ were very sensitive to noise where these functions were small. In these regions, in order to calculate N as expressed by Eq. 12 or the time average of h, hand extrapolations were made for $\lambda(t)$ and $h(t)$. These extrapolations never represented more than 5% of the total N.

As a control for the validity of the transient noise-analysis technique, we have applied our procedure to a set of simulated signals. Each signal was constructed from a Monte Carlo sample of bump initiation time points drawn from a time-dependent Poisson process, which led to superimposed bumps of fixed time course, and with the bump amplitude given by a specified function of initiation time. The three time functions for the Poisson rate process, bump time course, and bump amplitude were all of the form $at^n \exp(t/\tau)$, with a time offset relative to the rate and an added dark value for the amplitude. The parameter values chosen spanned the ranges of those that emerged from our laboratory results. From these simulations, the bump's integer exponent, n, was always recovered correctly, and the bump decay time, τ, was recovered to within 10%. The total number of bump events was always recovered without major error and to within 10% in two-thirds of the cases, and the same was true of the average bump amplification factor over its dark value. The separation of the maxima of rate and amplitude was also recovered reasonably, to within 10 ms in most cases and without substantial systematic error. In summary, these simulations validated our method of transient noise analysis.

RESULTS

Flashes of light were delivered to dark-adapted ventral photoreceptor cells of *Limulus*, as described in the Methods section, and voltage-clamped responses were recorded. Both the amplitudes of the responses and their areas exhibited a supralinear dependence on light intensity. In Fig. 2 we show the responses of one cell to I_1 and $I_{1.5}$ (plotted downward by convention). One can note that although $I_{1.5}$ is only about three times I_1, its response has about eight times the amplitude. The response of $I_{1.5}$ is shorter in duration than that to I_1, but its area (time integral) is still about five times the area of the I_1 response.

This can be seen better in Fig. 3. Here the area of the response divided by the estimated number of bumps in the response is plotted as a function of light intensity. Constant quantum efficiency is assumed for this calculation. (This assumption turns out in fact to be valid; see below.) One sees that the response area per bump is higher by a factor of 2.5 at the highest intensity than for isolated bumps. If one assumes that the response is indeed composed of bumps, there are three possible explanations for this supralinearity: (*a*) more bumps than expected appear in the response to higher light intensities; that is, the quantum efficiency is higher; (*b*) the bumps have higher amplitudes during the response to the higher intensities; and (*c*) the bumps have longer durations. Alternative *c* is not negated by the observation that the total response has a shorter duration, because this could be caused by a decrease in the width of the bump latency distribution. In order to decide among these alternatives,

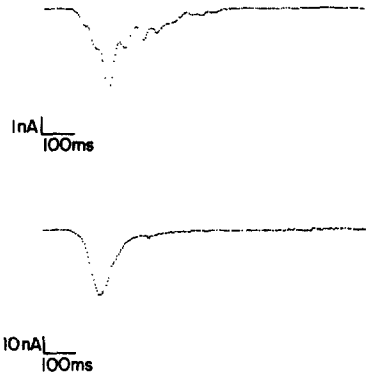

FIGURE 2. Typical flash responses at two light intensities. Top: $I_1 = 10I_0$; bottom: $I_{1.5} = 31.6I_0$, where I_0 induced about two bumps. The start of each trace is the time of delivery of flashes of duration 5 ms. Note that the lower response is eight times higher in amplitude and five times larger in area (time integral) than the upper response, for an increase in intensity of a factor of only 3.16 (supralinearity).

the noise analysis described in the Theory section was used to determine the rate, amplitude, and duration of the bumps comprising the responses.

In Fig. 4, three consecutive responses to the I_1 flashes are shown as examples of the data on which the noise analysis was performed. All the other figures presented in this article refer to the same cell as in Fig. 4. Very similar results were obtained in three other cells. In each cell, 50 light flashes were delivered at each intensity. The first step in the analysis is to calculate the decompound power spectrum (Eq. 11). The result for the $I_{1.5}$ intensity in this cell is indicated in Fig. 5. The solid line is the fit of a curve of the type described in Eq. 14, which corresponds to a time course for the bump as given in Eq. 13. The fact that the bump time course does not change very much with intensity can be seen in Fig. 6. In this figure, we compare the normalized mean time course of isolated bumps seen at the I_0 intensity with the bump time course calculated from Eq. 13 for the I_1 intensity. The parameters of the bumps for I_1 were always close to those of $I_{1.5}$. The time course of the I_0 bump is similar to, though slightly narrower and more symmetrical than, the derived time course of the I_1 bump. This result is an indication that in this relatively small range of low light intensities, the bump time course on the average is not strongly dependent on intensity.

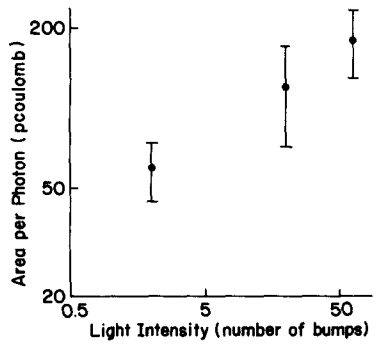

FIGURE 3. The area of the flash response has a supralinear dependence on light intensity; that is, the response area per absorbed photon increases with increasing light intensity in a certain range. The logarithmic intensity scale on the abscissa is based on a direct count of the average number of bumps elicited by the weakest flashes, with the other points plotted at values that are this number multiplied by the factor of increase in intensity. This will be the actual mean number of bumps in the flashes of these intensities if the quantum efficiency is constant. The linear ordinate is the flash area divided by the nominal flash intensity in numbers of bumps. All points are averages of four cells. The error bars indicate standard errors.

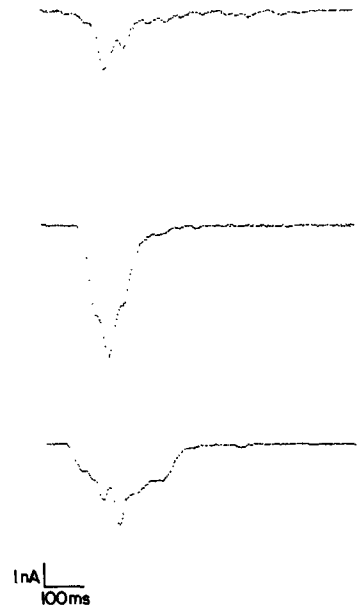

FIGURE 4. Response variability. Three successive responses to brief flashes are shown. The traces begin at the time of the flashes. The stimulus intensity was I_1, and stimuli were delivered every 30 s. Note the large difference among the responses, assumed in this article to be due to their being composed of different numbers of bumps appearing at random times.

There remains the possibility that the time course varies during the course of the response. In order to look for such a trend, the responses were divided into sections and T_{bump} was calculated for each section as described above. Fig. 7 sets out the results, which show that the bump duration is quite constant during the response. We conclude that changes in the bump duration are not responsible for the supralinearity of the dependence of the response area on intensity.

The next step in noise analysis was to calculate the temporal behavior of the rate, $\lambda(t)$, and mean amplitude, $h(t)$, of the bumps by using Campbell's theorem, in the forms given by Eqs. 20 and 21. For this purpose, we extracted from the signals the mean and the variance of the response. They are plotted for the $I_{1.5}$ intensity in Fig. 8. The left-hand plot is the mean, R, and the right-hand plot is the variance, V, as functions of time, where $t = 0$ is the time of delivery of the flash.

The functions $\lambda(t)$ and $h(t)$ were calculated from the mean and variance by using Eqs. 20 and 21 and in Fig. 9 they are plotted for both intensities and all cells. Since h and λ derive from the ratio of two noisy functions at the early and late times, where the terms in Eqs. 20 and 21 are small, h and λ are very noisy, and therefore are not plotted, at these times. The left-hand plot for each intensity is the rate λ as a function

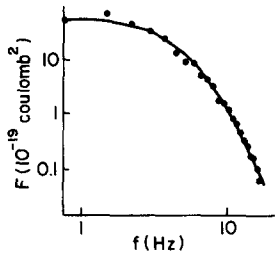

FIGURE 5. The decompound power spectrum F (see text). Both scales are logarithmic. This spectrum was obtained for cell 1 at the $I_{1.5}$ intensity. The dots are the experimental points and the solid line is a fit of a curve as described in Eq. 14, with parameters $n = 2$ and $\tau = 24$ ms.

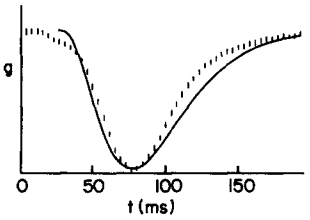

FIGURE 6. Normalized bump time courses. The continuous line is the bump shape as calculated from the decompound power spectrum at the I_1 intensity for cell 1. It represents the curve described in Eq. 13 with parameters $n = 2$ and $\tau = 22$ ms. The vertical bars are the averages of 10 isolated bumps recorded at the I_0 intensity with their times of steepest rise made to coincide. Note that the two time courses are quite similar, though the I_1 bump is slightly broader and more asymmetrical.

of time. Because the stimulus was a brief flash, λ represents the bump latency distribution. There is an initial delay, followed by a rapid rise and a slower decline. The latency distribution is sensitive to the light intensity, the delay, and maximum move to shorter times as the intensity is increased. The mean values of the observed latencies, peak positions, and distribution widths of the λ curves are given in Table I for the two intensities. The area under the $\lambda(t)$ curve is the total number, N, of bumps in the response, and will be used in Fig. 10 (see Eq. 12). For the purpose of evaluating the integral, the values of λ were extrapolated smoothly to zero at longer times. The central result of this study is illustrated in the right-hand plots of Fig. 9, which display the time course of the mean bump amplitude $h(t)$. After some delay, h increases strongly during the course of the response, reaches a maximum, and begins to decline. Table I shows the average over four cells of the latencies of the curves, their peak positions, their widths, and their maximum and mean values. The mean increase factor was calculated by weighting the value of h according to λ.

We conclude that the supralinearity in flash responses arises primarily from an

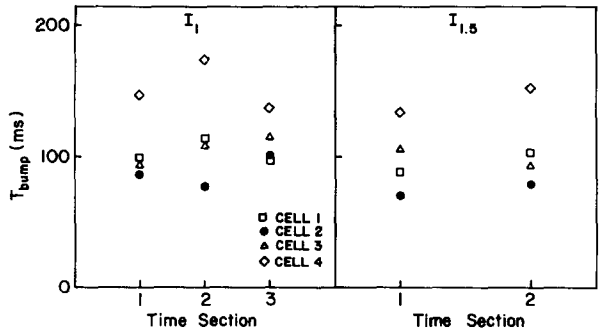

FIGURE 7. Constancy of bump duration during the course of a flash response. The durations (Eq. 17) of the bump averaged within each of three or two equal sections (low and high intensity, respectively) of the flash response are displayed. There is no indication of a trend with time in the bump duration. The power spectra for each cell are also very similar in the five cases.

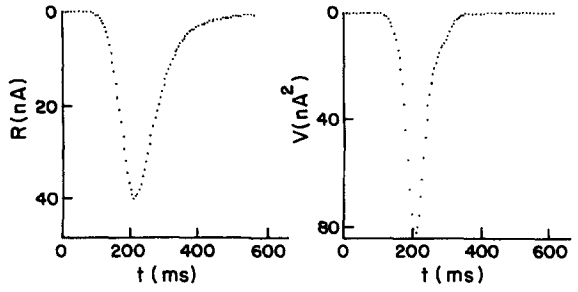

FIGURE 8. Time courses of the mean, R, and variance, V, of the flash responses of cell 1 at the $I_{1.5}$ intensity. These were calculated from 50 responses similar to the ones shown in Fig. 4 but for this intensity. The variance was drawn downward in order to make easier the comparison with the mean time course.

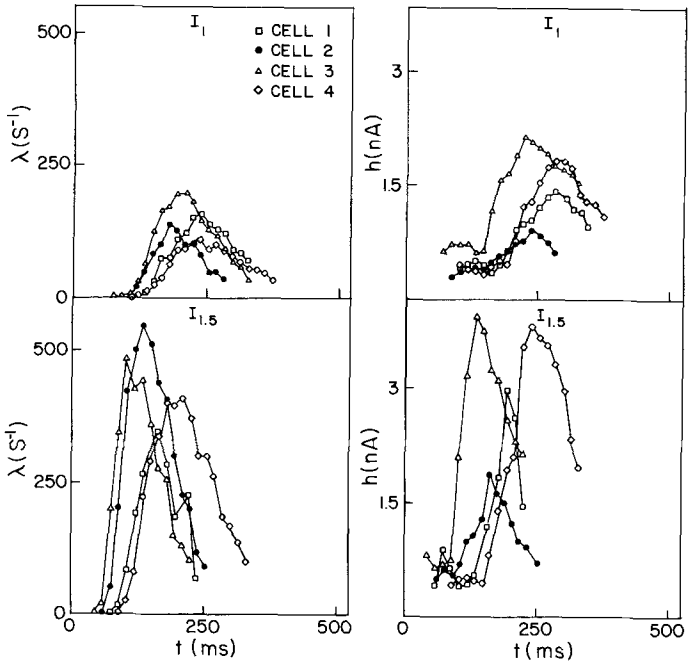

FIGURE 9. The time courses of the mean rate, λ, and the mean amplitude, h, of the bumps during a flash response. These were calculated from the results shown in Fig. 8 and similar results for the other cells by using Eqs. 20 and 21. $\lambda(t)$ gives the bump latency distribution. After a delay, it rises quickly to a maximum and falls more slowly back to baseline. Its area is the number of bumps, N, in the response, and this number will be used in Fig. 10. Note that $h(t)$, after some delay, strongly increases during the course of the response, before declining late in the response. Since the bump duration does not change appreciably during the response (Fig. 7), the increase in bump amplitude constitutes the main correlate of the supralinear dependence of response area on intensity. The results are displayed for four cells and two light intensities. The values of various parameters read off these curves are given in Table I.

TABLE I

Flash Response Characteristics

Variable	R			λ		h	
Intensity	I_0	I_1	$I_{1.5}$	I_1	$I_{1.5}$	I_1	$I_{1.5}$
Area	0.12±0.03	2.41±0.97	11.3±3.2				
Number of bumps	2.0±0.13	20.0±2.6	54±5				
Average bump height	0.51±0.09	0.97±0.26	1.75±0.40				
Time to peak		299±18	236±25	219±15	153±22	263±17	190±22
Width		145±8	122±8	134±8	111±10	170±15	106±19

The values of various parameters of the flash responses and their derived properties. Durations and times are in milliseconds; times refer to bumps beginning at those times after the flash presentation; widths are full widths at half-height. Response areas are in nanocoulombs and bump amplitudes, h, are in nanoamperes. λ is the bump rate per second. The numbers are averages over four cells. The errors are standard errors.

increase in bump size during the response, and not significantly from increases in either bump duration or quantum efficiency. In order to illustrate this conclusion, we display in Fig. 10, as a function of the intensity, the average bump amplitude; the total number, N, of bumps in the flash response, divided by intensity; and the integrated response area, also divided by intensity. The ordinate scales are normalized to make the points coincide at the I_0 intensity. One sees that the response supralinearity is indeed very largely due to the increase in the average bump amplitude. The total

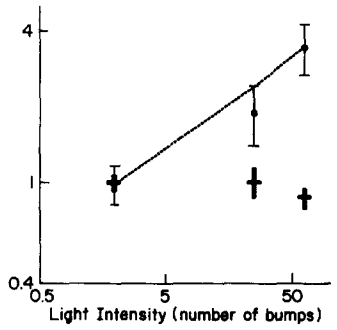

FIGURE 10. The intensity dependence of the average bump amplitude (filled circles), the total number N of bumps in the flash response per unit flash intensity (plus signs), and the integrated response area per unit light intensity (dotted line). The ordinate scales are all normalized to unity at the I_0 intensity. The logarithmic abscissa scale is the same as in Fig. 3. One can see that the response supralinearity correlates quantitatively with the increase in average bump amplitude. The total number of bumps in the response per unit light intensity is constant, corresponding to constant quantum efficiency. The error bars and the vertical lengths of the crosses indicate standard errors.

number of bumps in the response is linear with light intensity, which indicates the constancy of the quantum efficiency.

DISCUSSION AND CONCLUSIONS

In this study, we have investigated changes in the properties of the bumps that underlie the responses to flashes of light in the regime in which these responses exhibit a supralinear dependence on light intensity. Since the signal amplitude changes significantly during the course of one of the elementary bumps of which it is composed, standard techniques of noise analysis cannot be applied. For this purpose, we therefore developed a new technique, which is described in detail in the Theory section. We note that our technique of analysis differs from that of Sigworth (1980, 1981*a*, *b*) and is addressed to a different situation: his technique is specialized to rectangular bumps of constant amplitude but of stochastic duration, while our approach treats bumps with complex but causal shape and variable amplitude. The approach of Wong et al. (1974) is similar to ours but more restricted in that it is based on the approximation that the signal changes slowly compared with the elementary event, so that the signal can be considered to be a succession of steady states.

The comment should be made that one can propose chemical-chain transducers that incorporate a fast-acting nonlinearity and for which the immediate application of Campbell's theorem is inappropriate. A chain that involves n-fold cooperativity at some forward step is such an example. Such models yield a power spectrum whose shape depends on mean output level at low intensity: this feature is not seen in our data (Fig. 7 and its legend). Furthermore, these models yield systematic errors dependent on the output level when Campbell's theorem is applied directly to the data for determination of quantum efficiency. These errors would lead to a discrepancy between the calculation from Campbell's theorem and the result of a direct count of bumps in a low-intensity record; our data show no such discrepancy (Fig. 10). Accordingly, we believe that the chain contains no nonlinearity strong and fast enough to disturb the conclusions of this article.

Application of our method to the responses to flashes in dark-adapted cells leads to the following conclusions about the four parameters that characterize the quantal composition of the responses: the amplitude, quantum efficiency, latency, and duration of the component bumps. The bump amplitude exhibits a strong increase during the course of the response, followed by a decline. (The implications of this time course will be discussed below.) Prior (or continuing) illumination has previously been reported to increase the bump amplitude slightly at very low intensities (Stieve and Bruns, 1980) and to decrease the bump amplitude strongly at higher intensities (Dodge et al., 1968; Wong et al., 1982). The quantum efficiency is constant against the intensity of the flashes, as it is in the steady state (Wong et al., 1982). However, very weak prior illumination has been reported to increase quantum efficiency (Stieve and Bruns, 1980), while higher intensities apparently decrease quantum efficiency (Srebro and Behbehani, 1972). Mutation (Minke, 1982) and abnormal pharmacological media (Corson et al., 1983) may also change the quantum efficiency. (A new phenomenon that may be interpreted as a modulation either of quantum efficiency or of latency has been reported by Grzywacz et al., 1985, but the observation has not

yet been analyzed in detail.) There is a substantial decrease in bump latencies and latency dispersion with increasing flash intensity. Prior illumination also decreases bump latency (Martinez and Srebro, 1976; Stieve and Bruns, 1980; Wong et al., 1980). The bump duration is constant through the flash response. It is also less dependent on intensity (if at all) than is the latency. In the steady state as well, the duration is less dependent on intensity than the latency (Wong et al., 1982), and the mechanism might be similar. In addition, it is possible that the mechanism responsible for the reduction in duration sets in slowly compared with the flash response duration.

These data provide the quantal basis for several observed nonlinearities in the responses of photoreceptors. The supralinearity of flash responses correlates largely or entirely with an increase in the bump amplitude. The sublinearity that corresponds to light adaptation correlates largely with a decrease in the bump amplitude, but with a contribution from the bump duration (Dodge et al., 1968; Wong, 1978). The acceleration of the response with increasing intensity correlates largely with a decrease in bump latency. The acceleration of the early phase of the response is of particular interest (Payne and Fein, 1986; also see Hamdorf and Kirschfeld, 1980, for a related observation in the fly), and here the latency decrease is the exclusive correlate, since the bump amplitude has not yet begun to change (Fig. 9). The acceleration of the response by prior illumination (Fuortes and Hodgkin, 1964; French and Kuster, 1985; but see Stieve et al., 1983, for a contrary observation) also appears to be ascribable to a latency decrease. We comment that the study of Lisman and Brown (1975) reports data consistent with our own: at a comparable flash intensity, they show a latency reduction and also a response peak that follows an ~ 1.2 power of intensity. Similarly, Brown and Coles (1979) show an ~ 1.5 power before the regime of adaptation.

We shall now discuss what can be learned about the mechanism of bump amplitude enhancement from the time courses of the bump parameters. In analyzing these time courses, we first note that the response is the product of the bump rate, λ, and the bump amplitude, h, folded with the bump time course, g [$R = (\lambda \cdot h) * g$]. Accordingly the peak of $\lambda \cdot h$, which will be roughly halfway between the peaks of λ and of h, should precede that of R by approximately the time from the start of a bump to its centroid (remember that the time axes of λ and h refer to the times at which the bumps begin). In fact, the peaks of λ and h occur 80 and 40 ms, respectively, before that of R (Table I). Thus, the peak of $\lambda \cdot h$ is at ~ 60 ms, while the time from the bump to its centroid is ~ 70 ms, in reasonable agreement. This consideration means that the peak position data provide values for only two independent parameters; let us assign them to the position of the R peak and the separation of the λ and h peaks. We shall not consider further the R position here, but comment only on the λ-h separation.

As a framework model for our discussion, we start with the suggestion by Grzywacz and Hillman (1985), based on their observations on isolated bumps, that the transduction process at this level can be described as a chain of first-order enzymatic reactions. Onto this model we graft a single nonlinear stage to explain the bump amplitude enhancement: either a cooperativity in which an enzyme in the chain acts cooperatively to produce the next-stage material, or a positive feedback or feedforward loop in which an accessory material created at some stage of the chain acts as a

cofactor, perhaps cooperatively, of the enzymatic reaction at another stage in the chain.

We now suggest that the data exclude a mechanism of cooperativity. The argument starts with placing an upper limit on the duration of the stage on which the enhancement acts. A continuously acting enhancement must, in principle, modify the time course of the bump. We have calculated that if the enhancement acted on a stage whose duration was that of the final bump response, the durations of bumps occurring in the last segment of the flash response would be reduced by 40% compared with those in the first segment. This is outside the acceptable limits supplied by Fig. 7. We conclude that the duration of the bump at the stage of the chain on which the enhancement acts cannot be more than 30–40 ms (and therefore must precede the final stage). It is clear that the separation in the peaks of λ and h arising from cooperativity in one stage cannot be greater than the duration of that stage, and this is borne out by analysis. That is, if the duration of that stage is very short, the effect amounts simply to a nonlinear dependence of h on λ, with no peak separation. However, we have used the observed λ curves to show that a λ-h peak separation arising from cooperativity in fact cannot be more than ~40% of the duration of the enhancement stage—that is, not more than ~16 ms, in disagreement with the observations.

We conclude that the mechanism of the bump enhancement is a positive feedback or feedforward loop. We have analyzed simple examples of these two cases. In the simpler feedforward case, the λ-h separation is roughly the difference in the direct and side path times from the source of the feedforward material to the point at which it acts. For instance, if the feedforward material acts on a point 20 ms further along the chain via a loop whose length is 60 ms, the h peak will lag the λ peak by ~40 ms. For a particular class of simple models, these considerations apply exactly to the λ-h centroid separation.

The feedback case is more complicated because of its reflexive nature. We find that the h peak can in principle be postponed as much as one wishes by increasing the feedback gain, as long as any λ signal remains, and that this delay also depends on intensity. Within a simple model, we are able to obtain the observed λ-h separation with the observed degree of enhancement. As a mechanism for bump amplitude enhancement, a positive feedback loop has a potential for explosion, while a positive feedforward does not. However, we have shown (Grzywacz and Hillman, 1988) that adaptation is probably a negative-feedback loop and that the positive-feedback explosion can be avoided if the source of the positive feedback is later in the chain than the sink (point of action) of the negative feedback.

A final note about the time course of h: The decline of h before the end of the response can be ascribed either to a decline in the enhancement mechanism or to the onset of the adaptation mechanism. The time at which the decline begins ranges from 120 to 300 ms in different cells and at different intensities. These times span those suggested by Lisman and Brown (1975) and Fein and Charlton (1977) for the onset of adaptation. We conclude that the decline may well arise from the onset of adaptation, and that we then have no information on the offset time of the enhancement. The onset latency of the enhancement is ~40 ms from the start of the response and 90–170 ms from the flash.

The above statements constitute strong constraints on possible models for bump phototransduction. What follows is a scheme that satisfies all these constraints. The scheme is an arbitrary choice out of several that appear to be conceptually close to minimal.

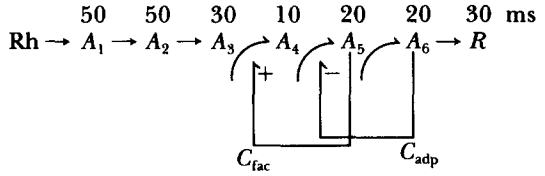

(Scheme I)

In this scheme, the portion A_1–A_3 is non-amplifying, and determines the bump latency and latency spread. Materials A_3, A_4, and A_5 are enzymes for producing the succeeding stages from substrates and are responsible for the bump amplitude and time course. Accessory materials C_{fac} and C_{adp} are created by A_5 and A_6 (their "sources") and act as a cooperative cofactor and inhibitor of the A_3 and A_4 reactions, respectively. A_6 can be amplifying or non-amplifying. Rh and R are rhodopsin and the response of the system (open ion channels), respectively. Each number in the upper row represents the lifetime of the state below it. The numbers derive from a variety of considerations and are very rough. The facilitatory feedback is assumed to be fast, while the adaptation feedback must involve a delay of 60–80 ms in order to explain the late onset of adaptation in the flash response.

The basic chain of the model, a series of non-amplifying stages followed by a series of amplifying stages, appears to be required by data on the latency and time course distributions of the bumps comprising the responses (Wong et al., 1980; Tiedge, 1981). The relevant observations are the brevity of the bump duration compared with its latency, the large latency spread, the time course of the bump itself, and the independence of the changes in latency and time course under varying conditions. Insertion into such a chain of two nonlinear molecular processes, one responsible for the flash supralinearity and the other for light adaptation, leads to a limited number of formally distinguishable models (see Grzywacz and Hillman, 1988) involving feedbacks, feedforwards, and local processes. If one imposes on these models the available constraints, one is left with only a small number of possibilities.

The addition of state A_6 preceding the response is called for by evidence in *Limulus* and *Calliphora* that at least part of the adaptive material arises from a stage preceding the response. In *Limulus*, Lisman (1976) has shown that at least part of the Ca^{++} apparently responsible for adaptation arises from intracellular stores. Furthermore, Lisman and Strong (1979) demonstrated that this release is not activated by ions flowing through channels. The release of Ca^{++} from intracellular stores must therefore depend on a step prior to channel opening. Moring et al. (1979) showed that in *Calliphora* a flash stimulus can depress the response to a prior flash even before its own response begins to develop, so again the adaptation must arise from a stage preceding the response.

Fein and DeVoe (1973) observed that the state of adaptation in this preparation is "functionally independent" of membrane potential. (Kleinschmidt and Dowling,

1975, made a similar observation in gecko.) This result may be consistent with our model if one assumes that the feedback materials are long-lived and so accumulate and partly integrate the response.

In summary, we have applied a new technique of dynamic noise analysis to the transient responses of *Limulus* ventral photoreceptors following brief flashes of 20–50 effective photons, and we reach several conclusions. The phenomenon of response area supralinearity is due to a light-induced increase in the amplitude of the underlying quantum bump, as quantum efficiency and bump duration are essentially independent of flash intensity in this range. Within the response, the peak in the bump amplitude lags that of the bump rate by ~40 ms; this observation, in conjunction with a substantially smaller change in the bump duration (if any) over the time course of the flash response, strongly constrains the possible arrangement of chemical mechanisms whose combined action gives rise to phototransduction.

APPENDIX

In this appendix, we develop the equations used in the text, which follow from the four assumptions advanced in the Theory section. This inquiry addresses probabilistic questions of some depth and must involve a notation sufficiently elaborate to describe both the biophysical situation and our various manipulations on the data.

Our whole theoretical approach follows from two considerations: first, the laboratory yields us an unpredictable current signal, $J(t)$, from which we can average, over many repeated runs, algebraic combinations yielding, for example, $\langle J(t)J(t')\rangle$, where the two current values are correlated if the two times are close together; and second (from assumption 2: uncorrelated elementary events), the probabilistic current signal can be regarded as the sum of uncorrelated probabilistic pieces:

$$J(t) = \sum_s J_s(t), \tag{A1}$$

which, though they overlap in time, originate from events that occur independently in short disjoint time intervals $(\Delta t)_s = t_s - t_{s-1}$.

All the moments of a random variable X [such as $J(t)$ at fixed t] are subsumed in its characteristic function:

$$C_X(\alpha) = \langle \exp \alpha X\rangle = \left\langle \sum_{n=0}^{\infty} \frac{1}{n!} \alpha^n X^n \right\rangle = \sum_{n=0}^{\infty} \frac{1}{n!} \langle X^n\rangle \alpha^n, \tag{A2}$$

and similarly all the joint moments of two correlated random variables X and Y [such as $J(t)$ and $J(t')$] are subsumed in their joint characteristic function

$$C_{X,Y}(\alpha, \beta) = \langle (\exp \alpha X)(\exp \beta Y)\rangle = \sum_{\substack{m=0 \\ n=0}}^{\infty} \frac{1}{m!} \frac{1}{n!} \langle X^m Y^n\rangle \alpha^m \beta^n. \tag{A3}$$

We make the further formal observation that if either of these characteristic functions (each has 1 as its leading constant term) is substituted into the series for the logarithm

$$\ln (1 + u) = u - \tfrac{1}{2} u^2 + \tfrac{1}{3} u^3 \ldots \tag{A4}$$

the result is straightforward to organize as a power series:

$$G_X(\alpha) = \ln \langle \exp \alpha X\rangle = \sum_{n=1}^{\infty} G_X^{(n)} \alpha^n$$

and (A5)

$$G_{X,Y}(\alpha, \beta) = \ln \langle (\exp \alpha X)(\exp \beta Y) \rangle = \sum_{\substack{m=1 \\ n=1}}^{\infty} G_{X,Y}^{(m,n)} \alpha^m \beta^n,$$

where each coefficient ($G_x^{(n)}$ or $G_{X,Y}^{(m,n)}$) is a specific algebraic combination of moments. In particular, we calculate

$$G_X^{(1)} = \langle X \rangle, G_X^{(2)} = \tfrac{1}{2} (\langle X^2 \rangle - \langle X \rangle^2), G_{X,Y}^{(1,1)} = \langle XY \rangle - \langle X \rangle \langle Y \rangle; \tag{A6}$$

whence we recognize $G_X^{(1)}$ as the mean, $G_X^{(2)}$ as half the variance about the mean $\langle (X - \langle X \rangle)^2 \rangle$; and $G_{X,Y}^{(1,1)}$ as the covariance about the means of the correlated X and Y, $\langle (X - \langle X \rangle) \cdot (Y - \langle Y \rangle) \rangle$.

Step A5 has a particular payoff if the variable X is the sum of uncorrelated random variables [as $J(t)$ is according to Eq. A1]. Say $X = X_1 + X_2$; then

$$C_{X_1+X_2}(\alpha) = \langle (\exp \alpha X_1)(\exp \alpha X_2) \rangle = \langle \exp \alpha X_1 \rangle \langle \exp \alpha X_2 \rangle = C_{X_1}(\alpha) \cdot C_{X_2}(\alpha), \tag{A7}$$

whence its logarithm A5 yields

$$G_{X_1+X_2}(\alpha) = G_{X_1}(\alpha) + G_{X_2}(\alpha); G_{X_1+X_2}^{(n)} = G_{X_1}^{(n)} + G_{X_2}^{(n)} \tag{A8}$$

for each n and by a calculation exactly similar to A7

$$G_{X_1+X_2,Y_1+Y_2}^{(m,n)} = G_{X_1,Y_1}^{(m,n)} + G_{X_2,Y_2}^{(m,n)}$$

for each m, n. The generalization to a larger sum as in A1 is immediate.

Evidently this machinery can be used to evaluate the expressions in the text, which are called

$$R(t) = \langle J(t) \rangle \tag{A9}$$

$$V(t) = \langle (J(t) - R(t))^2 \rangle \tag{A10}$$

$$K(t_1, t_2) = \langle (J(t_1) - R(t_1))(J(t_2) - R(t_2)) \rangle, \tag{A11}$$

respectively, the time-dependent ensemble mean of the current, ensemble variance of the current, and two–time-dependent covariance of the current. Straightforward procedures lead to text Eqs. 1, 2, and 8, which express these experimentally measured functions in terms of the underlying elementary processes that determine the probability distribution of $J(t)$.

First we consider the situation in which the bump amplitude, $h(t)$, is a sure (nonrandom) function of the experiment time t. The time course of a bump that starts at time t_s is given by $g(t - t_s)$. The rate of independent (Poisson) events we call $\lambda(t)$. We may ask: what is the probability distribution of that part of the current that arises in a very brief time interval $(\Delta t)_s$ between two time marks t_{s-1} and t_s, which we choose closely spaced? We can think of the fixed time t at which this contribution $J_s(t)$ is measured as later than the brief time interval in which the contribution arises. If the interval $(\Delta t)_s$ is chosen to be brief enough, the probability that one event occurs in $(\Delta t)_s$ will be small and that of two events will be negligible, so we can write

$$P_0 = \text{Prob}(J_s(t) = 0) = 1 - \lambda(t_s)(\Delta t)_s, \tag{A12}$$

$$P_1 = \text{Prob}(J_s(t) = h(t_s)\, g(t - t_s)) = \lambda(t_s)(\Delta t)_s \tag{A13}$$

whence

$$\begin{aligned} C_{J_s(0)}(\alpha) &= P_0 \exp(\alpha \cdot 0) + P_1 \exp\left(\alpha \cdot h(t_s) \cdot g(t - t_s)\right) \\ &= \left(1 - \lambda(t_s)(\Delta t)_s\right) + \lambda(t_s)(\Delta t)_s \cdot \exp\left(\alpha \cdot h(t_s) \cdot g(t - t_s)\right) \\ &= 1 + (\Delta t)_s \cdot \lambda(t_s) \cdot \{-1 + \exp\left(\alpha \cdot h(t_s) \cdot g(t - t_s)\right)\}. \end{aligned} \tag{A14}$$

In the logarithm formula A4, we can again ignore powers of $(\Delta t)_s$ higher than the first, and at once calculate

$$G_{J_s}(t)(\alpha) = (\Delta t)_s \cdot \lambda(t_s) \cdot \{-1 + \exp\left(\alpha \cdot h(t_s) \cdot g(t - t_s)\right)\}. \tag{A15}$$

We now exploit the fact that $J(t)$ is the sum of uncorrelated pieces $J_s(t)$ (A1) and we also exploit the sum property of the log-characteristic function A8:

$$\begin{aligned} G_{J(0)}(\alpha) &= \sum_s (\Delta t)_s \cdot \lambda(t_s) \cdot \{-1 + \exp\left(\alpha \cdot h(t_s) \cdot g(t - t_s)\right)\} \\ &= \int dt' \lambda(t') \cdot \{-1 + \exp\left(\alpha \cdot h(t') \cdot g(t - t')\right)\}. \end{aligned} \tag{A16}$$

If this expression is represented as a power series in α, the coefficient of α^1 is the mean $\langle J(t) \rangle$, while twice the coefficient of α^2 is the variance around the mean as we saw above at A6. These coefficients can be isolated in the usual way by differentiation; thus,

$$\langle J(t) \rangle = G^{(1)}_{J(0)} = \left(\frac{\partial}{\partial \alpha} G_{J(0)}(\alpha)\right)\Big|_{\alpha=0} = \int dt' \lambda(t') h(t') g(t - t'), \tag{A17}$$

which is exactly the expression for $R(t)$ given in Eq. 1 of the main text. Similarly, application of $\partial^2/\partial\alpha^2$ to A16, followed by $\alpha = 0$, would isolate the variance about the mean according to A6, but the variance is also a special case of the covariance evaluated below.

We note that if $h(t_s)$ is a further independent random variable, the analysis above still goes through for every narrow subrange of h. Because of the property (A8) of additivity from independence, we can add over these subranges, which yields the mean value of $h(t')$ in A17, which is also its meaning in text Eq. 1.

The evaluation of the covariance $K(t_1, t_2) = G^{(1,1)}_{J(t_1),J(t_2)}$ is equally straightforward. If an event in fact takes place in $(\Delta t)_s$ [with probability $P_1 = \lambda(t_s)\,(\Delta t)$] then both $J_s(t_1)$ and $J_s(t_2)$ will be given by $J_s(t)$ in A13, whence

$$\begin{aligned} C_{J_s(t_1),J_s(t_2)}(\alpha, \beta) = \{&1 - \lambda(t_s) \cdot (\Delta t)_s + \lambda(t_s) \cdot (\Delta t)_s \\ &\cdot \exp\left(\alpha \cdot h(t_s) \cdot g(t_1 - t_s)\right) \cdot \exp\left(\beta \cdot h(t_s) \cdot g(t_2 - t_s)\right)\} \end{aligned} \tag{A18}$$

and proceeding as we did to A16

$$G_{J(t_1),J(t_2)}(\alpha, \beta) = \int dt' \lambda(t') \{1 - \exp\left(\alpha \cdot h(t') \cdot g(t_1 - t')\right) \cdot \exp\left(\beta \cdot h(t') \cdot g(t_2 - t')\right)\} \tag{A19}$$

from which

$$K(t_1, t_2) = \left(\frac{\partial^2}{\partial\alpha\partial\beta} G_{J(t_1),J(t_2)}\right)\Big|_{\substack{\alpha=0 \\ \beta=0}} = \int dt' \lambda(t') \left(h(t')\right)^2 g(t_1 - t') g(t_2 - t'). \tag{A20}$$

As we argued in the paragraph that followed Eq. A17, if h is a further independent random variable, its square in Eq. A20 will be replaced by its mean square, and if h is exponentially

distributed, then $\langle h^2 \rangle = 2\langle h \rangle^2$. If we change notation and let $h(t)$ stand for the mean of an exponentially distributed random bump amplitude, then this factor 2 is introduced in Eq. A20, which becomes identical to text Eq. 8. If we now let $t_1 = t_2 = t$ [and remember $g(t-t')$ is causal and hence is nonzero for t' only up to t], we get text Eq. 2 for the time-dependent variance. For the remainder of this appendix, we write $\bar{h}$ for the (time-dependent) mean value of the exponentially distributed height variable, and introduce the factor of 2, which arises because $2\bar{h}^2$ is the mean-square height.

The "decompound power spectrum" of the main text can now be calculated. It is straightforward to evaluate the two-time Fourier transform of $K(t_1, t_2)$ in text Eq. 8 (or A20) to obtain the function of two angular velocities:

$$F(\omega, \theta) = \int dt_1 \int dt_2 e^{-i\omega t_1} e^{-i\theta t_2} K(t_1, t_2) = 2\lambda \widetilde{\bar{h}^2}(\omega + \theta) \cdot \tilde{g}(\omega) \cdot \tilde{g}(\theta). \tag{A21}$$

For the particular choice $\theta = -\omega$, this reduces to

$$F(\omega, -\omega) = 2\lambda \widetilde{\bar{h}^2}(0) \cdot |\tilde{g}(\omega)|^2, \tag{A22}$$

which is text Eq. 9 for the decompound power spectrum of the signal J.

Finally, we point out that if we truncate the signal at a time T', making the signal zero for all times after T', the development for the autocovariance for all the times $t_1, t_2 < T'$ is unchanged, and the autocovariance is zero if $t_1 > T'$ or $t_2 > T'$. In that case, if one takes the double Fourier Transform in the pathway $\omega = -\theta$, the result is:

$$F_{T'}(\omega, -\omega) = 2 \int_{-\infty}^{T'} \lambda(t) \bar{h}^2(t) \, | \sim g^{T'-t}(\omega) \, |^2 \, dt, \tag{A23}$$

where $|\tilde{g}^{T'-t}(\omega)|^2 = \int_{-\infty}^{T'-t} \int_{-\infty}^{T'-t} e^{i\omega(t_1'-t_2')} g(t_1') g(t_2') \, dt_1' \, dt_2'$. For all times that $T' - t > \Delta$, where Δ spans the effective decay of the bump $g(t)$, we get, effectively, $|\tilde{g}^{T'-t}(\omega)| = |\tilde{g}(\omega)|^2$. Then

$$F_{T'}(\omega, -\omega) = 2\left(\int_{-\infty}^{T'-\Delta} \lambda(t) \bar{h}^2(t) \, dt |\tilde{g}(\omega)|^2 + \int_{T'-\Delta}^{T'} \lambda(t) \bar{h}^2 |\tilde{g}T'-t(\omega)|^2 \, dt \right). \tag{A24}$$

Thus if a much larger portion of the response occurs before $T' - \Delta$ than between $T' - \Delta$ and T', the second integral can be neglected and the truncated decompound power spectrum will be proportional to $|\tilde{g}(\omega)|^2$. The same analysis holds just as well for a section of the signal between T' and a second time T'' as for a section from T' to ∞.

N. M. Grzywacz and P. Hillman thank the Neurosciences Institute (New York) for hospitality during preparation of this manuscript.

This work was supported by a grant from the United States Israel Binational Science Foundation (BSF), Jerusalem, and by grant EY-1428 from the U.S. National Institutes of Health to B. Knight.

Original version received 23 June 1986 and accepted version received 28 October 1987.

REFERENCES

Adolph, A. 1964. Spontaneous slow potential fluctuations in the *Limulus* photoreceptor. *Journal of General Physiology.* 48:297–322.

Adolph, A. 1968. Thermal and spectral sensitivities of discrete slow potentials in *Limulus* eye. *Journal of General Physiology.* 52:584–599.

Bayer, D., and R. B. Barlow, Jr. 1978. *Limulus* ventral eye. Physiological properties of photoreceptor cells in an organ culture medium. *Journal of General Physiology.* 72:539–563.

Baylor, D. A., T. D. Lamb, and K. W. Yau. 1979. Responses of retinal rods to single photons. *Journal of Physiology.* 288:613–634.

Brown, J. E., and J. A. Coles. 1979. Saturation of the response to light in *Limulus* ventral photoreceptor. *Journal of Physiology.* 296:373–392.

Brown, J. E., H. Harary, and A. Waggoner. 1979. Isopotentiality and an optical determination of series resistance in *Limulus* ventral photoreceptors. *Journal of Physiology.* 296:357–372.

Calman, B. G., and S. C. Chamberlain. 1982. Distinct lobes of *Limulus* ventral photoreceptors. II. Structure and ultrastructure. *Journal of General Physiology.* 80:839–862.

Capovilla, M., L. Cervetto, and V. Torre. 1983. The effects of phosphodiesterase inhibitors on the electrical activity of toad rod. *Journal of Physiology.* 343:277–294.

Clark, A. W., R. Millecchia, and A. Mauro. 1969. The ventral photoreceptor cells of *Limulus.* I. The microanatomy. *Journal of General Physiology.* 54:289–309.

Cooley, J. W., and J. W. Tukey. 1965. An algorithm for the machine calculation of Fourier series. *Mathematical Computation.* 19:297–301.

Corson, D. W., A. Fein, and W. W. Walthall. 1983. Chemical excitation of *Limulus* photoreceptors. II. Vanadate, GTP-γ-S, and fluoride prolong excitation evoked by dim flashes of light. *Journal of General Physiology.* 82:659–677.

DeVoe, R. D. 1972. Dual sensitivities of cells in wolf spider eyes at ultraviolet and visible wavelengths of light. *Journal of General Physiology.* 59:247–269.

Dodge, F. A., B. W. Knight, and J.-I. Toyoda. 1968. Voltage noise in *Limulus* visual cells. *Science.* 160:88–90.

Fain, G. L., and J. E. Lisman. 1981. Membrane conductances of photoreceptors. *Progress in Biophysics and Molecular Biology.* 37:91–147.

Fein, A., and J. S. Charlton. 1977. Enhancement and phototransduction in the ventral eye of *Limulus. Journal of General Physiology.* 69:553–569.

Fein, A., and R. D. DeVoe. 1973. Adaptation in the ventral eye of *Limulus* is functionally independent of the photochemical cycle, membrane potential, and membrane resistance. *Journal of General Physiology.* 61:273–289.

French, A. S., and J. E. Kuster. 1985. Nonlinearities in locust *Locusta migratoria* during transduction of small numer of photons. *Journal of Comparative Physiology.* A156:645–652.

Fuortes, M. G. F. 1959. Discontinuous potentials evoked by sustained illumination in the eye of *Limulus. Archives Italiennes de Biologie.* 97:243–250.

Fuortes, M. G. F., and A. L. Hodgkin. 1964. Changes in time scale and sensitivity in the ommatidia of *Limulus. Journal of Physiology.* 172:239–263.

Fuortes, M. G. F., and S. Yeandle. 1964. Probability of occurrence of discrete potential waves in the eye of the *Limulus. Journal of Physiology.* 47:443–463.

Graham, C. H., and H. K. Hartline. 1935. The responses of single visual sense cells to lights of different wave lengths. *Journal of Physiology.* 18:917–931.

Grzywacz, N. M., and P. Hillman. 1985. A test of linearity of the transduction process in photoreceptors: *Limulus* passes, others fail. *Proceedings of the National Academy of Sciences.* 82:232–235.

Grzywacz, N. M., and P. Hillman. 1988. Biophysical evidence that light adaptation in *Limulus* ventral photoreceptors is due to a negative feedback. *Biophysical Journal.* 53:337–348.

Grzywacz, N. M., P. Hillman, and B. W. Knight. 1985. A study of the bump rate transfer function in *Limulus* photoreceptors. *Investigative Ophthalmology and Visual Science.* 26:113. (Abstr.)

Hamdorf, K., and K. Kirschfeld. 1980. "Prebumps": evidence for double-hits at functional sub-units in a rhabdomeric photoreceptor. *Zeitschrift fur Naturforschung.* 35c:173–174.

Hanani, M., and P. Hillman. 1976. Adaptation and facilitation in the barnacle photoreceptor. *Journal of General Physiology.* 67:235–249.

Katz, G. M., and T. C. Schwartz. 1974. Temporal control of voltage-clamped membranes: an examination of principles. *Journal of Membrane Biology.* 17:275–291.

Kirschfeld, K. 1965. Discrete and graded receptor potentials in the compound eye of the fly (*Musca*). *In* The Functional Organization of the Compound Eye. C. G. Bernhard, editor. Pergamon Press, Elmsford, NY. 291–307.

Kleinschmidt, J., and J. Dowling. 1975. Intracellular recordings from Gecko photoreceptors during light and dark adaptation. *Journal of General Physiology.* 66:617–648.

Laughlin, S. B., and P. G. Lillywhite. 1982. Intrinsic noise in locust photoreceptors. *Journal of Physiology.* 332:25–45.

Lillywhite, P. G. 1977. Single photon signals and transduction in an insect eye. *Journal of Comparative Physiology.* 122:189–200.

Lisman, J. E. 1976. Effects of removing extracellular Ca^{++} on excitation and adaptation in *Limulus* ventral photoreceptors. *Biophysical Journal.* 16:1331–1335.

Lisman, J. E., and J. E. Brown. 1975. Light-induced changes of sensitivity in *Limulus* ventral photoreceptors. *Journal of General Physiology.* 66:473–488.

Lisman, J. E., G. L. Fain, and P. M. O'Day. 1982. Voltage-dependent conductances in *Limulus* ventral photoreceptors. *Journal of General Physiology.* 79:187–209.

Lisman, J. E., and J. A. Strong. 1979. The initiation of excitation and light adaptation in *Limulus* ventral photoreceptors. *Journal of General Physiology.* 73:219–243.

Martinez, J. M., II, and R. Srebro. 1976. Calcium and the control of discrete wave latency in the ventral photoreceptor of *Limulus*. *Journal of Physiology.* 261:535–562.

Mauro, A., E. Kaplan, and S. Poitry. 1982. Light-induced voltage fluctuations in the photoreceptors of barnacles and the honeybee drone. *Biophysical Journal.* 37:A197. (Abstr.)

Millecchia, R., and A. Mauro. 1969. The ventral photoreceptor cells in *Limulus*. III. A voltage-clamp study. *Journal of General Physiology.* 54:331–351.

Minke, B. 1982. Light-induced reduction in excitation efficiency in the *trp* mutant of *Drosophila*. *Journal of General Physiology.* 79:361–386.

Moring, J., M. Jarvilehto, and K. Moring. 1979. The onset of light adaptation in the visual cells of the fly. *Journal of Comparative Physiology.* A132:153–158.

Neher, E., and C. F. Stevens. 1977. Conductance fluctuations and ionic pores in membranes. *Annual Reviews of Biophysics and Bioengineering.* 6:345–381.

Nygaard, R. W., and T. E. Frumkes. 1982. LEDs: convenient, inexpensive sources for visual experimentation. *Vision Research.* 22:435–440.

Payne, R., and A. Fein. 1986. The initial response of *Limulus* ventral photoreceptors to bright flashes. Released Ca^{++} as a synergist to excitation. *Journal of General Physiology.* 87:243–269.

Rice, S. O. 1944. Mathematical analysis of random noise. *Bell Telephone System Journal.* 23:282–332.

Rushton, W. A. H. 1961. The intensity factor in vision. *In* Light and Life. W. D. McElroy and H. B. Glass, editors. The Johns Hopkins University Press, Baltimore, MD. 706–722.

Scheid, F. 1968. Numerical Analysis. McGraw-Hill, Inc., NY. 235–266.

Scholes, J. 1965. Discontinuity of the excitation process in locust visual cells. *Cold Spring Harbor Symposium on Quantitative Biology.* 30:517–527.

Sigworth, F. J. 1980. The variance of sodium current fluctuations at the node of Ranvier. *Journal of Physiology.* 307:97–129.

Sigworth, F. J. 1981*a*. Covariance of nonstationary sodium current fluctuations at the node of Ranvier. *Biophysical Journal.* 34:111–133.

Sigworth, F. J. 1981*b*. Interpreting power spectra from nonstationary current fluctuations. *Biophysical Journal.* 35:289–300.

Smith, T. G., Jr., J. L. Barker, B. M. Smith, and T. R. Colburn. 1980. Voltage clamping with microelectrodes. *Journal of Neuroscience Methods.* 3:105–128.

Srebro, R., and M. Behbehani. 1972. Light adaptation of discrete waves in the *Limulus* photoreceptor. *Journal of General Physiology.* 60:86–101.

Stieve, H., and M. Bruns. 1980. Dependence of bump rate and bump size in *Limulus* ventral nerve photoreceptor on light adaptation and calcium concentration. *Biophysics of Structure and Mechanism.* 6:271–285.

Stieve, H., and M. Bruns. 1983. Bump latency distribution and bump adaptation of *Limulus* ventral nerve photoreceptor in varied extracellular calcium concentration. *Biophysics of Structure and Mechanism.* 9:329–339.

Stieve, H., M. Bruns, and H. Gaube. 1983. The intensity dependence of the receptor potential of the *Limulus* ventral nerve photoreceptor in two defined states of light and dark adaptation. *Zeitschrift fur Naturforschung.* 38c:1043–1054.

Takeda, T. 1982. Discrete potential waves in the photoreceptors of a gastropod mollusc, *Hermissenda crassiconis. Vision Research.* 22:303–309.

Tiedge, J. 1981. Deterministiche und stochastiche Modelltheorien zur Photorezeption des Pfeilschwanzkrebes, *Limulus polyphemus.* Ph.D. Thesis, Aachen University.

Ventura, D. F., and N. M. Puglia. 1977. Sensitivity facilitation in the insect eye. *Journal of Comparative Physiology.* 114:35–49.

Walther, J. B. 1965. Single cell responses from the primitive eyes of an annelid. *In* The Functional Organization of The Compund Eye. C. G. Bernhard, editor. Pergamon Press, Elmsford, NY. 329–336.

Wong, F. 1978. Nature of light-induced conductance changes in ventral photoreceptors of *Limulus. Nature.* 276:76–79.

Wong, F., and B. W. Knight. 1980. The adapting-bump model for eccentric cells of *Limulus. Journal of General Physiology.* 76:539–557.

Wong, F., B. W. Knight, and F. A. Dodge. 1974. Transient behavior of the adapting-bump model parameters in the eccentric cell of *Limulus. Association for Research in Vision and Ophthalmology Abstracts.* 13.

Wong, F., B. W. Knight, and F. A. Dodge. 1980. Dispersion of latencies in photoreceptors of *Limulus* and the adapting-bump model. *Journal of General Physiology.* 76:517–537.

Wong, F., B. W. Knight, and F. A. Dodge. 1982. Adapting bump model for ventral photoreceptors of *Limulus. Journal of General Physiology.* 79:1089–1113.

Wu, C. F., and W. L. Pak. 1975. Quantal basis of photoreceptor spectral sensitivity of *Drosophila melanogaster. Journal of General Physiology.* 69:667–679.

Wu, C. F., and W. L. Pak. 1978. Light-induced voltage noise in the photoreceptor of *Drosophila melanogaster. Journal of General Physiology.* 71:249–268.

Yau, K. W., P. A. McNaughton, and A. L. Hodgkin. 1981. Effect of ions on the light-sensitive current in retinal rods. *Nature.* 292:502–505.

Yeandle, S. 1958. Evidence of quantized slow potentials in the eye of *Limulus. American Journal of Ophthalmology.* 46:82–87.

Yeandle, S., and J. B. Spiegler. 1973. Light-evoked and spontaneous discrete waves in the ventral photoreceptor of *Limulus. Journal of General Physiology.* 61:552–571.